1991

Numerical simulation of PBL depth during subsidence inversion conditions

George L. Fruehauf
San Jose State University

Order Number 1347153

Numerical simulation of PBL depth during subsidence inversion conditions

Fruehauf, George Lentz, M.S.

San Jose State University, 1991

U·M·I
300 N. Zeeb Rd.
Ann Arbor, MI 48106

NUMERICAL SIMULATION OF PBL DEPTH DURING SUBSIDENCE INVERSION CONDITIONS

A Thesis

Presented to

The Faculty of the Department of Meteorology

San Jose State University

In Partial Fulfillment

of the Requirements for the Degree

Master of Science

By

George L. Fruehauf

December 1991

APPROVED FOR THE DEPARTMENT OF METEOROLOGY

R. Bornstein

Douglas M. Lilly

Allen Becker

APPROVED FOR THE UNIVERSITY

Serena H. Stanford

ABSTRACT

NUMERICAL SIMULATION OF PBL DEPTH DURING SUBSIDENCE INVERSION CONDITIONS

by George L. Fruehauf

The URBMET three-dimensional planetary boundary layer (PBL) model has been modified to execute in a one-dimensional mode. Time varying PBL height was included as a new mesoscale process. Initial conditions now include a large scale inversion and a subsidence velocity profile. The magnitude of subsidence was determined via a new boundary condition on potential temperature at the model top.

Experiments using a time varying PBL height showed better results than those in which it was held constant. The subsidence velocity is necessary to sustain the subsidence inversion against surface convective effects and to effect the downward propagation of the large scale effects.

Dedicated to the Memory of My Father

ACKNOWLEDGMENTS

The author expresses thanks to Prof. R.D. Bornstein for his help and encouragement in bringing this work to completion. The valuable suggestions of Prof. D. Sinton and Mr. A. Becker are much appreciated. Special thanks go to David Ward for helping with the adaptation of the URBMET code to a CDC Cyber 170 machine. Finally, thanks go to Donna Hurth for sharing her word processing skills and always imparting cheerful inspiration.

TABLE OF CONTENTS

1. INTRODUCTION

Mesoscale and synoptic scale atmospheric models differ in the procedures used to initialize their wind and temperature fields (Pielke, 1984). With large scale flows, the wind is seldom far from gradient balance, indicating that the mass field dominates the response of the wind field. Thus, for these scales it is more important to measure the initial temperature distribution than the wind field. Temperatures are then used to obtain the mass field through the hydrostatic equation, with the distribution of mass represented by the pressure field. Initial winds are then diagnosed from the mass field.

Solutions at any level in such large scale models are almost independent of solutions at adjacent levels (Reuter, 1987) because of weak large scale vertical velocities, low levels of free atmospheric turbulence, and large vertical grid spacings. Solutions are thus quickly dominated by the upward propagation of the time and space varying surface boundary conditions. Initial model conditions are thus extremely important, and small differences may produce large differences in their solutions (Bengtsson et al., 1981).

As horizontal circulation scale is reduced, the relation between the wind and temperature (i.e., mass) fields

becomes more complex. The ratio of synoptic advection to the horizontal mesoscale pressure gradient can indicate whether the velocity or mass field dominates mesoscale circulation structure. Using scale analysis, Pielke (1984) gave this ratio as

$$I = \frac{U^2}{R\Delta T^*} , \qquad (1.1)$$

where all symbols are defined in the Appendix.

Over a heated mesoscale land mass under light synoptic flow, for example, I is less than unity. Thus the initial (and evolving) temperature distribution should be more important in the evolution of a planetary boundary layer (PBL) sea breeze circulation than would be the initial wind speed distribution.

Solutions at any level in such PBL models are extremely dependent on solutions at adjacent levels because of (relatively) large mesoscale vertical velocities, high PBL turbulence levels, and small vertical grid spacings. Solutions are also quickly dominated by the upward propagation of the time and space varying surface boundary conditions, and thus correct specification of initial conditions is not as important as it is with larger scale models.

A second reason for this lessened importance arises as air parcels at the upwind boundary of such models will normally advect out of the computational domain in a (relatively) few hours. Even though initial conditions in a mesoscale model have reduced importance, they are still best introduced in the most physically realistic and numerically consistent manner, especially if accurate model results for the first few simulated hours are required.

According to Pielke (1984), two methods have been used to initialize mesoscale meteorological models: objective analysis and dynamic initialization. Objective analysis normally involves multiple (when available) rawinsonde soundings. It consists of the interpolation of observed values to model grid points using weighting functions, in which grid values depend on distances to the observations (e.g., see Segal and Pielke, 1981). Within the field of objective analysis, an alternative to simple interpolation is the variational analysis technique of Sasaki (1970), in which one or more conservation relations are applied to minimize the variance of the differences between observations and extrapolated values.

Dynamic initialization consists of integrating model equations over a period of time to approximate a steady-

state dynamic balance and to damp data inconsistencies. To achieve a steady-state solution, lower boundary values of temperature and moisture are held constant.

An interesting meteorological situation for mesoscale modelers is a thermally driven circulation in a PBL capped by an elevated subsidence inversion. Previous attempts at including such inversions into model initialization procedures have not accounted for the general circulation scale subsidence that produces and sustains the inversion (e.g., Pielke, 1974). They have also not accounted for the horizontal divergence of the gradient flow necessary to maintain the downward vertical velocity.

Atmospheric PBL depth H during daytime hours can be defined as the minimum between the height H_c at which the vertical turbulent transfers of momentum, heat, and mass from the surface to the atmosphere first reach negligibly small values (Arya and Byun, 1985) and the height H_i of the base of an elevated capping inversion, which acts as a barrier to such vertical turbulent transfers. During the day H_c is referred to as the mixing layer (Yamada and Mellor, 1975), a layer of high turbulent intensity located above an unstable surface boundary layer (SBL). By contrast, the (nighttime) mixed layer is a layer of low intensity mechanical turbulence within a nearly laminar stable surface layer.

Knowledge of H has many applications; e.g., to air pollution meteorologists it is important in determining pollutant concentration patterns in time and space. To PBL modelers H_c is a necessary parameter in the determination of heat and momentum diffusivity profiles, e.g., as in the analytical formulation of O'Brien (1970).

Values of H_c can be estimated directly from acoustic echo soundings as the top of the first continuous echo layer, or from aircraft measurements as the top of the mixing layer, above which pollutant concentrations rapidly decrease. Estimates can also be obtained from theoretical relationships involving PBL turbulence parameters.

In some PBL models, H_c is set to an equal arbitrary constant (Estoque, 1961, 1962; Bornstein, 1975). The sea breeze model of Pielke (1974) included a variable (in time and space) H_c using the following formulation by Blackadar and Tennekes (1968):

$$H_c = 0.25(u_*/f) \quad , \tag{1.2}$$

where

$$f = 2\Omega\sin\phi \quad .$$

The parameter u_* can be determined by a PBL model (as described below). Note that (1.2) is valid only under neutral stability conditions.

The value of H_c in the three-dimensional mesoscale model of Anthes and Warner (1978) was defined simply as the level at which the potential temperature lapse rate exceeded the arbitrary value of 1.3°C/km. This approach constrains H_c to vertical grid levels, which near the top of many PBL models are widely separated.

Stability effects on mixed layer depth H_c during stable conditions were studied by Zilitinkevich (1972). Using PBL similarity theory, he obtained

$$H_c = c(u_* L/f)^{\frac{1}{2}} \quad , \tag{1.3}$$

where Monin-Obukhov length L is given by

$$L = \frac{u_*^2 \theta_a}{g k_0 \theta_*} .$$

Like u_*, the parameter θ_* can be determined from a PBL model. The constant c was previously determined experimentally as 2.0 (Zilitinkevich, 1970). The relationship shows that H_c decreases with increasing stability, as both L and u_* decrease.

Equation (1.3) has been used by others, but with values of c obtained by correlating observed and predicted values of H_c; e.g., Mahrt et al. (1982) used observed values of surface fluxes obtained by Melgarejo and Deardorff (1975) and found a value of 0.6. In general, correlation coefficients between observed and computed values of H_c from equation (1.3) are about 0.7 (Nieuwstadt, 1984a).

Using a value of $c = (k_0)^{\frac{1}{2}} = 0.6$ in equation (1.3), Yu (1978) studied H_c over a wide range of stable stratifications using data from the Wangara experiment (Clarke et al., 1971). For slightly stable conditions he obtained a high correlation (0.93) between observed and calculated H_c values, while for extremely stable conditions the correlation was only 0.40.

The one-dimensional nocturnal PBL model of Nieuwstadt (1984b) was closed by assuming a constant (with height and time) value of the SBL flux Richardson number R_{if}. This produced the following expression for c:

$$c = (\sqrt{3}\, k_0 R_{if})^{1/2}, \tag{1.4}$$

where R_{if} is related to the gradient Richardson number R_i by:

$$R_{if} = \frac{K_0}{K_m} R_i = \frac{g(\partial\theta/\partial z)}{\theta_a(\partial V/\partial z)} \frac{K_0}{K_m} . \qquad (1.5)$$

Using a value of 0.2 for the observed limiting constant value of R_{if} under stable conditions at the 213m Caubauw tower, his value for c equaled 0.37. This value shows good agreement with the 0.4 obtained by both Brost and Wyngaard (1978) and Garratt (1982) from higher order turbulence closure models.

Barnum and Rao (1975) used a two-dimensional conservation equation for mixing layer depth H_c to study its variability during weak wind summer unstable daytime hours. The derivation for their prognostic equation for H_c involved integrating the thermodynamic energy equation over the mixing layer. To do so, the potential temperature lapse rate along the axis of the mean horizontal flow, as well as its temporal variation, were assumed constant. The temporal aspect of this constraint is not applicable for simulations throughout an entire day.

Deardorff (1974) proposed the following prognostic rate equation for mixing layer depth H_c under non-stable conditions:

$$\frac{dH_c}{dt} = w(H_c) + \frac{1.8(w_*^3 + 1.1u_*^3 - 3.3u_*^2 f H_c)}{g(H_c^2/\theta_0)(\partial\theta^+/\partial z) + 9w_*^2 + 7.2u_*^2} . \quad (1.6)$$

The effects of convection due to surface heating is included via the convective velocity w*, defined as:

$$w_* = \begin{cases} [[-g/\theta_0)u_* \theta_* H_c]^{1/3} , & \theta_* \leq 0 \\ 0 , & \theta_* > 0 . \end{cases} \quad (1.7)$$

This formulation is based on both numerical results from a sophisticated third order turbulence closure PBL model (Deardorff, 1974) and from laboratory studies (Deardorff et al., 1974). Comparison with observations showed that (1.6) accurately represented mixing layer growth during clear days.

Pielke and Mahrer (1975) used (1.6) in a three-dimensional numerical PBL model. Reasonable results were obtained simulating Day 33 of the Wangara Experiment, as it was described by Clarke et al., (1971). Likewise Segal et al. (1982) used (1.6) in the same PBL model, and simulated daytime mesoscale atmospheric processes over the Cheasapeak Bay area. Predicted mixing layer heights were, as expected, consistently higher over land than offshore, where the sur-

face layer was thermally stable. Strong gradients of H_c were observed at the coast in the morning; however, due to advection, the gradient weakened with time as daytime PBL heights over the water increased.

Previous PBL models have specified steady-state synoptic conditions and simulated deviations from them, i.e., the development of non-steady PBL circulations. The current research describes modifications made to the three-dimensional PBL model described by Bornstein et al. (1986, 1987). Non-steady large scale influences are now included in the model via a specified time varying upper boundary temperature. A steady large scale subsidence velocity is also included; this allows for vertical advective effects on the temperature field (as well as on the moisture and vorticity fields). The magnitude of this velocity is determined so as to make it consistent with the observed lapse rate within the subsidence inversion. The model is also modified to accommodate a time varying PBL height.

2. MODEL FORMULATION

Time dependent PBL depth calculations have been made using a modified version of the URBMET PBL model described by Bornstein et al. (1986, 1987). For this study, the original three-dimensional model was modified to execute over homogeneous terrain in a one-dimensional mode to study the effects (e.g., vertical advection) of an elevated subsidence inversion on PBL structure. This involved development of a modified initialization scheme, and of a new non-steady variable H(t) scheme. In the new scheme, the time variation of PBL depth H(t) is generally given as the minimum between the lowest elevated inversion base height $H_i(t)$ and the theoretically calculated mixing depth $H_c(t)$.

The URBMET model was previously used in a one-dimensional mode by Diertele (1979) and Santhanam (1980), and in a two-dimensional mode by Bornstein (1975), Bornstein and Robock (1976), MacCraken and Bornstein (1977), Bornstein and Runca (1977), and Reichenbacher and Bornstein (1979). In all previous studies, URBMET assumed a constant value of H throughout a given simulation. In addition, these studies utilized uniform initial potential temperature and moisture profiles, as well as a zero large scale subsidence velocity.

The URBMET model consists of two atmospheric layers: a constant-flux surface layer of depth h, in which mean field variables are analytic, and an upper transition layer to a height of Ht in which the hydrodynamic (vorticity) and thermodynamic (potential temperature and specific humidity) equations describing atmospheric transport are solved numerically by finite-differences.

The transition-layer equations were derived from the exact equations of motion for a viscous, Newtonian fluid in a rotating coordinate system. A set of restrictions was imposed on these equations by assuming that: the atmosphere is Boussinesq and hydrostatic; turbulence can be described by eddy coefficients (via O'Brien, 1970); sub-saturation vapor concentration is a conserved property; and that radiative flux divergence occurs only from naturally occurring gases.

In the constant-stress SBL, friction scaling quantities (e.g., u_*) are assumed constant with height; however, they may change with time due to changing atmospheric stability conditions. The Businger et al. (1971) formulation is used to obtain flux profile relationships. Soil processes are included through a finite-differenced soil layer, following the formulation of Sasamori (1970) and Diertele (1979).

Boundary condition at the deepest grid point within the soil layer assumes constant values for temperature and moisture. At the surface, no slip boundary flow conditions apply, while energy and moisture balance equations are used to predict $\theta(t)$ and $q(t)$, respectively (following Santhanam, 1980). Zero and first order continuity are assumed for all variables at the internal boundary at the top of the SBL, i.e., at h. At the model top H_t, the wind is geostrophic with a zero shear.

a. Initialization

The dynamic initialization scheme produces an equilibrium consistent one-dimensional horizontal wind field for a well mixed unsaturated layer capped by a large scale subsidence inversion. The sub-inversion layer is initially neutral with a constant (with height) moisture distribution, while the inversion layer initially has a constant potential temperature gradient and moisture content to the model top. The initialization procedure requires input upper boundary values of a steady state geostrophic wind velocity V_g, moisture, and potential temperature.

These values can be obtained via an objective analysis from a rawinsonde sounding or from predicted vertical profiles from a larger scale numerical model; the former ap-

proach is used in the current study. With an additional rawinsonde sounding at the same site, but at a different time, a steady subsidence velocity profile $w_s(z)$, consistent with the above input profiles, is then obtained (as described below).

Step 1. Determine neutral PBL depth, H

The initial estimate of H is the minimum between the input parameter H_i and the value of H_c, obtained from the following relationship of Blackadar (1962):

$$H_c = 0.01V_g/f \quad . \tag{2.1}$$

Step 2. Determine analytical Ekman spiral

The u and v components of V in a one-dimensional Ekman type layer are given, respectively, by

$$u(z) = u_g[(1-\exp(-az)\cos(az) - v_g\exp(-az)\sin(az)] \quad , \qquad z \leq H_c \tag{2.2}$$

and

$$v(z) = u_g[\exp(-az)\sin(az) + v_g[(1-\exp(-az)\cos(az)] \quad , \quad z \leq H_c \quad ,$$

where

$$a = (f/2K_m)^{\frac{1}{2}}$$

$$u_g = V_g \cos\alpha$$

$$v_g = V_g \sin\alpha \quad .$$

The constant eddy viscosity coefficient K_m in the above Ekman spiral is given by Blackadar (1962) as

$$K_m = 0.5H^2 f/\pi^2 \quad . \tag{2.3}$$

For grid levels above H_c, the wind velocity V is initially set equal to V_g.

Step 3. Determine numerical equilibrium wind profile

A numerical equilibrium wind profile under neutral conditions is obtained above the SBL, up to the computational grid point below the model top (i.e., $h < z < H_t$). The solution is obtained from the finite-difference analog (given in Bornstein et al., 1987) to the following PBL equation of motion

$$\frac{\partial V}{\partial t} = f(V - V_g)xk + \frac{\partial}{\partial z}(K_m \frac{\partial V}{\partial z}) \, , \tag{2.4}$$

where the eddy viscosity profile $K_m(z)$ is the analytical O'Brien (1970) function, dependent on wind shear, mixing layer depth, and surface roughness. During this phase of the initialization procedure, the value of H_c is no longer given by (2.1), but by the following expression from Blackadar and Tennekes (1968):

$$H_c(t) = 0.33u_*/f \quad , \tag{2.5}$$

where friction velocity u_* is obtained by the PBL model from the following continuity constraint on V at the top of the analytical SBL:

$$\frac{V(3h/2) - V(h/2)}{\Delta z} = \frac{\partial V}{\partial z} \quad . \tag{2.6}$$

Given the logarithmic wind speed profile for a neutral SBL,

$$V(z) = (u_*/k_0)\ln[(z+z_0)/z_0) \quad , \quad 0 \leq z \leq h \quad , \tag{2.7}$$

the vertical speed-shear is given by

$$\frac{\partial V}{\partial z} = \frac{u_*}{k_0(z+z_0)} \quad . \tag{2.8}$$

When the above two expressions are used in (2.6), along with the known wind speed value from the first numerical finite-difference grid level above the SBL (i.e., at 3h/2), it can be shown that

$$u_* = \frac{k_0(h + z_0)V(3h/2)}{h + (h + z_0)\ln[(0.5h + z_0)/z_0]} \quad . \tag{2.9}$$

Thus as V(3h/2) changes with time during this phase of the initialization procedure, u_* changes, as does H_c.

The wind during this phase at each level undergoes a damped inertial oscillation, with a period $\tilde{\tau}$, given by

$$\tilde{\tau} = 2\pi/f \quad . \tag{2.10}$$

Equilibrium is assumed to have been achieved when, after several inertial periods, the maximum value of temporal variations of V in the computational domain over several hours is less than a prescribed value.

Step 4. Introduce subsidence inversion

Values of potential temperature θ within the elevated subsidence inversion (which extends to the model top H_t) are determined using an observed constant (with height) poten-

tial temperature gradient τ. The methodology used to obtain the input values of τ and H_i is described below.

The following upper boundary condition on θ is applied:

$$\frac{\partial \theta}{\partial t} = \dot{\theta} \quad , \; z = H_t \quad , \tag{2.11}$$

where the warming rate $\dot{\theta}(H_t)$ is a specified constant value, as determined from values from a large scale meteorological model or from two sequential rawinsonde soundings.

Thermal energy conservation in a horizontally homogeneous unsaturated PBL capped by a subsidence inversion is given by

$$\dot{\theta} = - w_s \frac{\partial \theta}{\partial z} + \frac{\partial}{\partial z}\left(K_0 \frac{\partial \theta}{\partial z}\right) + \dot{Q}(z) \tag{2.12}$$

where

$$\dot{Q} = - \frac{1}{c_p} \frac{\partial Q_n}{\partial z} \quad .$$

If turbulent heat diffusion within an inversion is assumed negligible (Cederwall, 1980), applying (2.12) at H_t yields an equation for the subsidence velocity w_s at that level, i.e.,

$$w_s = \frac{\dot{Q}_L - \dot{\theta}}{\gamma} \quad , \; z = H_t \quad , \tag{2.13}$$

where the inversion layer potential temperature gradient $\tau(H_t)$ and local potential temperature tendency $\dot{\theta}(H_t)$ are known input parameters. Radiative heating $\dot{Q}(H_t)$ is assumed equal to long wave radiative flux divergence $\dot{Q}_L(H_t)$, because it is greater than the magnitude of its short wave counterpart. The magnitude of $\dot{Q}_L(z)$ is evaluated in URBMET from radiative transfer equations using the known $\theta(z)$ and $q(z)$ profiles, as described by Bornstein et al. (1987).

Application of (2.13) requires a steady-state value of $\dot{Q}_L(H_t)$, which implies a steady-state vertical gradient for Q_L at H_t. Since the value of $\dot{Q}_L$ at the finite-difference grid point below H_t changes (as θ and q at this level change), the value of $\dot{Q}_L$ at the boundary grid point above H_t is specified to change at the same rate. Application of (2.13) also requires a steady state value for the input parameter $\tau(H_t)$.

These assumptions produce a value for the large scale subsidence velocity at the model top $w_s(H_t)$ consistent with the heating imbalance ($\dot{\theta}$) between the large scale subsidence warming ($-w_s\tau$) and the atmospheric long-wave radiative temperature change ($\dot{Q}_L$). The radiative cooling is a

function of $\theta(z)$ and $q(z)$, both of which arise from an interaction between mesoscale and large scale effects.

Since the radiative term will be negative and τ is positive, to obtain a negative value for $w_s(H_t)$, i.e., subsiding motion, $\dot{\theta}(H_t)$ must be greater than (the negative) $\dot{Q}_L(H_t)$, i.e., it must be less negative or positive.

The (assumed steady state) values of $w_s(z)$ are specified uniform above the initial input inversion base H_0 and to linearly decrease to zero at the surface, i.e.,

$$w_s(z) = \begin{cases} w_s(H_t) , & z \geq H_0 \\ w_s(H_t)(z/H_0) , & z < H_0 . \end{cases} \qquad (2.14)$$

Equations (2.13) and (2.14) allow for a height variation of subsidence velocity consistent with the observed subsidence inversion potential temperature gradient, thus allowing large scale effects to be included in a PBL model. The large scale $w_s(z)$ will intensify and lower the base of an elevated inversion, which is also affected from below by mesoscale diffusion effects. Omission of this term produces erroneously rapid daytime inversion lifting rates.

b. Simulation

In the (neutral PBL) initialization phase, H_c was given by (2.5); during the simulation phase, it is given either by (1.6) during non-stable SBL conditions ($R_i \leq 0$) or by a modified version (described below) of (1.3) during stable SBL conditions ($R_i > 0$).

Stability within the SBL is evaluated from the finite-difference analog to the SBL Richardson number R_i for the layer from the surface to the first finite-difference grid point at 3h/2, i.e.,

$$R_i(3h/4) = \frac{1.5gh[\theta(3h/2)-\theta(h/2)]}{\theta_a[V(3h/2)-V(h/2)]^2} . \qquad (2.15)$$

Daytime convective processes cause H_c to increase, as parameterized by (1.6), whose finite-differenced analog is

$$Hc^{n+1} = H^n \qquad (2.16)$$

$$+ \Delta t \left[w_s(H^n) + \frac{1.8(w_*^3 + 1.1u_*^3 - 3.3u_*^2 fH^n)}{\frac{g(H^n)^2 r^+}{\theta_0} + 9w_*^2 + 7.2u_*^2} \right] ,$$

where required turbulence variables (w_* and u_*) are produced by URBMET. The value of $w_s(H^n)$ is a linearly interpolated value, while the potential temperature lapse rate above H^n,

given by $\tau+$, is evaluated (following Pielke, 1975) using θ-values at the two grid levels above H^n, i.e., from

$$\tau^+ = (\theta_{k+1} - \theta_k)/(z_{k+1} - z_k) \ . \qquad (2.17)$$

Time step magnitude Δt is determined using the time splitting method of Bornstein and Robock (1977). Previously calculated H (and not H_c) values are used in (2.16), consistent with the definition of H (i.e., it is the minimum of H_c and H_i). Note that H_i can only have values equal to heights of vertical grid levels.

When R_i becomes positive, the value of H_c is computed from a modified version (1.3), i.e., from

$$H_c = ((\sqrt{3}\ k_0 R_{if}\ u_* L)/f)^{1/2}, \qquad (2.18)$$

where values of variables in the above equation are again produced by URBMET at each timestep. In the derivation of his steady state model, which included (1.3) and (1.4), Nieuwstadt (1984b) had to assume that R_{if} remained constant with time. As URBMET predicts changes of R_{if} with time, better prediction of $H_c(t)$ is expected with (2.18) than from his model.

The night to day transition from (2.18) to (2.16) requires a special definition of H. Instead of the minimum

criteria, H is set equal to the current value of H_c. During this transition period, as surface heating is initiated, the SBL becomes non-stable and H_c values should rise; however, a (low-based) elevated inversion also forms. Thus, if the minimum criteria were used, H would decrease rather than increase after sunrise. This exceptional case terminates when H_i becomes greater than H_c, and the minimum criteria is again used.

With the onset of nighttime conditions, the surface source of turbulence is terminated. A new (relatively) shallow layer of low intensity turbulence is created near the ground. The upper part of the PBL (i.e., the mixed layer) becomes decoupled from the surface, and the previously existing daytime turbulence within it decreases quickly with time to negligible values. As soon as the SBL R_i becomes positive, the value of H_c previously given by (2.16) is determined by (2.18). This creates an instantaneous drop of $H_c(t)$; similar behavior also results with higher order turbulence closure schemes (Yamada and Mellor, 1975). This temporal discontinuity does not adversely affect results from the current model, as shown below.

The O'Brien (1970) formulation used in the current model specifies that K(z) profiles decrease to a minimum

value at the "top" of either the daytime thermal mixing layer or the nighttime mechanical mixing layer. In the current formulation, the top of the PBL H is taken as the minimum between H_i and H_c. Use of H (instead of H_c) as the "top" in the O'Brien equation produces an incorrect behavior of H_i during daytime convective periods following nighttime stable periods, as described below.

During stable periods H_i frequently decreases to a value below H_c, as subsidence overcomes surface induced convection. If H is then set equal to H_i and used as the "top" of the O'Brien K-profile, H_i will be unable to rise during the following daytime unstable period, because turbulent mixing will only extend up to H_i (and not beyond). It is therefore necessary to always use H_c as the top of the O'Brien profile. This means that a polluted PBL may extend to H_i concurrently with a mixing layer H_c that could extend to a somewhat greater depth. Of course, the mixing would act to cause H_i to approach H_c.

3. DATA PREPARATION

Cases selected for simulation were chosen to display meteorological conditions reproducible by both the new and existing model features, and to avoid physical processes not included in the current model. An appropriate case study must contain a well defined large scale subsidence inversion extending to a height greater than the typical daytime PBL depth (i.e., at least to 1.5km). This is necessary because the initial inversion top is taken as the model top in the current formulation. Local advective effects should be minimal, as the model is used in a one-dimensional mode; flat homogeneous terrain is thus ideal.

To test the $H_c(t)$ scheme, simulations should take place over land and not water, as diurnal temperature variations and convective heat fluxes are insignificant over water. Saturated mixing ratio values must be avoided, since the model atmosphere is assumed unsaturated. Clear skies are also necessary, as the model does not include cloud effects in its radiation transfer processes.

A synthesis of features appearing in two summers of slow rise rawinsondes from San Jose, CA. produced an idealized sounding. Such a sounding, rather than a single observed sounding, was used to initialize the model because it

was desired to test all the new physical processes in the model.

Two sequential (synthetic or real) temperature and dew point temperature rawinsonde soundings are required for the initialization procedure, with the later one used to determine the initial $\theta(z)$ and $q(z)$ profiles from which H_0 and H_t are determined. The earlier sounding is needed only to obtain a previous value of θ at H_t to calculate $\dot{\theta}(H_t)$ from

$$\dot{\theta} = \frac{\theta(t_2) - \theta(t_1)}{t_2 - t_1} \quad , \; z = H_t . \tag{3.1}$$

The height of the model top H_t is selected as the minimum between the height of the top of the subsidence inversion in the adjusted (see below) rawinsonde profile or 2000m. This is done because the current formulation assumes, via the omission of diffusion in (2.12), that surface effects do not extend to H_t.

The initial inversion base height H_0 is chosen as the level across which $q(z)$ decreases rapidly (Fig. 1). This level usually coincides with the height at which the temperature lapse rate becomes positive, thus defining the inversion base.

Specific humidity is then assumed to have unequal initially uniform values above and below H_0. These values are obtained from the initial rawinsonde sounding as the best fit (equal area) mixing ratio lines through the inversion and sub-inversion layers.

The temperature profile $T(z)$ below H_0 is smoothed to be dry adiabatic by an equal area technique. Within the inversion, $T(z)$ is also smoothed to a uniform value by the same area technique.

If the time of the later sounding does not coincide with the desired model initialization time, the surface temperature value is adjusted by use of appropriate surface observations. A dry adiabat is then extended through the adjusted surface temperature until it intersects the sounding. A $\theta(z)$ profile is then obtained from the following PBL approximation:

$$\theta(z) = T(z) + \Gamma z \quad . \tag{3.2}$$

To determine the initial wind profile via (2.2), the required value of V_g is obtained by inspection from 850mb wind data. The vertical wind profile $w_s(z)$ is computed from (2.13) and (2.14), using the observed input values of $\dot{\theta}$, τ, H_0, and H_t, as well as the model produced value of $\dot{Q}_L(H_t)$.

4. RESULTS

Simulations were designed to sequentially evaluate the effects from each new physical processes in the model and to evaluate model sensitivity to certain input parameters. A list of input values assumed during each run is given in Table 1.

Run 1 includes all new physical processes, except that the diurnal potential temperature trend at the model top is set to zero. Run 2 is the same as Run 1, except that vertical advective effects are ignored, as w_s is set to zero. Run 3 has a variable PBL height, but omits a subsidence inversion. Run 4 reproduces the model in the original form in a one-dimensional mode (as in Bornstein et al., 1986). Run 5 is like Run 4, but with no radiative flux divergence.

Run 6 is like Run 1, but with a cooling rate at H_t. Its subsidence is thus smaller, via Eq. (2.14), than for Run 1 (Fig. 2). Run 7 has both a higher initial inversion base and a stronger cooling rate than in Run 1, both of which weaken w_s (Fig. 2). Run 8 is like Run 1, except for its higher H_i and weaker V_g.

Table 1. Summary of input data; see Appendix for definition of symbols.

Run	H	$\dot{\theta}_t$	$\tau(H_t)$	H_0	V_g	$\dot{Q}$	$-w_s(H_t)$
	(m)	(K/day)	(K/km)	(m)	(m/s)	(K/day)	(cm/s)
1	f(t)	0	7	450	7	ON	2.0
2	f(t)	0	7	450	7	ON	0.0
3	f(t)	0	0	>H_t	7	ON	0.0
4	1050	0	0	>H_t	7	ON	0.0
5	1050	0	0	>H_t	7	OFF	0.0
6	f(t)	-6	7	450	7	ON	1.0
7	f(t)	-9	9	800	7	ON	0.4
8	f(t)	0	7	800	4	ON	2.0

This final run investigates effects from reduced mixing on nighttime stable SBL formation.

For all runs, θ_0 was initially set to 26°C. Initial T(z) and q(z) profiles for runs with $H_0 < H_t$ are given in Fig. 1, while for runs with $H_0 > H_t$, these parameters were assumed uniform with height. Computed ws profiles for each run are shown in Fig. 2. Each run began at 1800 LST and lasted for 72 hours; however, results from only the final 24hr period are usually presented, as it takes several hours for model adjustment in the initialization procedure.

Run 1 includes all new physical processes, except that the diurnal potential temperature trend at the model top is zero. The resulting peak subsidence velocity of 2cm/s (Fig. 2) produced a merging of the elevated subsidence and nocturnal surface radiation inversions, as shown in the final simulated midnight T(z) (Fig. 3). Surface heating weakened this combined inversion through its lowest 150m, but it still extended to the surface at noon on the final day (Fig. 4).

The initial adjustment period for H during Run 1 lasted for about two hours of simulated time (Fig. 5), when H_i was less than H_c and H fell rapidly due to the large value of

w_s. During the next 18 hours, H_i was constant and still less than H_c; hence, H remained constant at a (grid point) value of 125m.

An abrupt rise in H after 20 hours occurred when H_i became zero, and H was determined by H_c. As H(t) was determined from the stable layer $H_c(t)$ equation during the final 50 hours of Run 1, it shows the expected diurnal pattern of (somewhat) higher daytime than nighttime values (Figs. 5 and 6). The two hour adjustment period for H(t) indicates the need for a new equilibrium phase within the current initialization procedure to allow for the $w_s(z)$ and $\theta(z)$ profiles to achieve equilibrium.

An adjustment period is also evident in predicted surface temperature values during the first few hours of Run 1 (Fig. 7). Afterwards, however, the expected nighttime cooling and daytime warming diurnal cycle is superimposed on an adiabatic warming trend (Figs. 7 and 8) associated with the subsidence.

Above H, however, temporal changes of T and θ are minimal (Fig. 9), as vertical turbulent mixing does not extend above Hc, where radiative flux divergence (cooling) almost perfectly balances subsidence (warming). The steady state near-neutral layer above the inversion top is thus inconsis-

tent with the steady-state upper inversion boundary condition, which therefore should be redefined. This inconsistency does not, however, adversely affect results within and below the inversion.

Surface relative humidity values (Fig. 10) for Run 1 show a longer adjustment period (20 hours). The final 50 hours do, however, show the expected lower daytime and higher nighttime diurnal trend again superimposed on slightly decreasing values (Figs. 10 and 11), associated with both the surface warming trend in Figs. 7 and 8 and the subsidence-induced downward advection of dry air.

Values of $H_c(t)$ under stable conditions are directly proportional to $u_*(t)$ via (2.18), and thus the variation of $u_*(t)$ during Run 1 (Fig. 12) is consistent with the corresponding H variation (Fig. 6). Predicted SBL R_i values for the final 24 hour period of Run 1 (Fig. 13a) show the expected diurnal variation (for a persistent stable surface based inversion), i.e., larger positive nighttime than positive daytime values, consistent with the previously discussed Run 1 variations of H, T_0, RH, and u_*.

Simulated K_θ profiles (Fig. 14) indicate a sensitivity to stability, as peak values (at all levels) occur at 1200 LST, when the SBL is least stable (Fig. 13a). Note that K_θ

is set equal to a small value at levels above H_c, i.e., above 150m.

Run 2 uses the same inputs as Run 1, except that vertical advective effects are ignored, as ws is set to zero (Table 1). Without advective warming, no warming trend occurs and lower T_0 values result, e.g., during the final 24 simulated hours the cooling relative to Run 1 is 6°C (Fig. 8). The Run 2 surface relative humidity diurnal cycle is like that of Run 1, but with consistently higher values (Fig. 11). The drying effects of subsidence in Run 1 is the cause of its lower values.

The subsidence inversion of Run 2 (not shown), initially equal to that of Run 1, weakens with time and never reaches the surface, as it did in Run 1. A large scale subsidence inversion cannot, therefore, be sustained over time against surface based convection effects without the vertical advective effects from its subsidence velocity.

Absence of the stabilizing effect of the omitted subsidence velocity produced a more typical diurnal cycle of SBL R_i values (Fig. 13a), i.e, positive at night and negative during daytime hours, of course, the positive nighttime values are smaller than those in Run 1. Omission of subsidence velocity allowed for significantly higher Run 2 daytime H

values (Fig. 6), as convective lifting effects were not opposed by subsidence. Nighttime H values were also somewhat higher due to increased mechanical turbulence levels associated with the decreased nocturnal stability.

Values of H in Run 2 were determined by H_c via (2.18) during nighttime stable conditions and via (2.16) during daytime unstable conditions. In both formulations, H_c is directly proportional to u_*, which in Run 2 is larger at all times than the corresponding values of Run 1 (Fig. 12), due to the deceased (day and night) stability of Run 2.

In Run 3, the subsidence inversion itself is also omitted (Table 1), producing uniform initial θ and q profiles. The SBL R_i thus now possesses the usual diurnal cycle, i.e., positive at night and negative during the day (Fig. 13a). The negative daytime R_i values cause H (equal to H_c) to be dominated by convective effects via (2.16). It thus reaches a value of 1062m at 1400 LST (Fig. 15), consistent with its large daytime u_* values (Fig. 12). The diurnal cycle of H now also more strongly reacts to the cycle of its surface temperature than in Runs 1 and 2 (Figs. 7 and 8), as daytime convection does not have to battle subsidence.

A weak cooling trend is superimposed on the T_0 diurnal cycle in Run 3 (Fig. 7). Its amplitude, however, decreases

with time, reaching near cyclic equilibrium on the third day of the simulation (Fig. 8).

At midnight on the final day of Run 3, a radiative surface based inversion did not form (Fig. 16) due to the high value of V_g. The weak elevated inversion at 200m is a mixing inversion at the PBL top (Fig. 15). Noontime surface warming produces a deep (900m) well mixed adiabatic layer (Figs. 15 and 17).

Surface relative humidity values (Fig. 10) of Run 3 show no adjustment period as in Run 1. The expected lower daytime and higher nighttime diurnal cycle of RH is superimposed on a slight positive trend.

Inclusion of a (large, 1050m) constant H in Run 4 produced unrealistically large nighttime heat diffusivities (Fig. 18). This unreasonably increased (relative to that of Run 3) nighttime mechanical turbulence levels, as parameterized by u_* (Fig 12).

The diurnal T_0 cycle was reproduced in Run 4 (Fig. 8), with values slightly elevated above those of Run 3. The constant value of H produces larger K_θ values (via the O'Brien formulation) during morning and nighttime hours.

This enhances diffusion to the surface, thus countering radiative flux divergence (cooling) effects.

The enhanced nighttime heat diffusion also affected the diurnal R_i cycle of Run 4 (Fig. 13a), which was similar to that of Run 3, except for its smaller positive nighttime values. This indicates less stable conditions, in agreement with the higher Run 4 nighttime values of T_0.

Effects on PBL structure from ignoring radiative flux divergence are tested in Run 5 (Table 1). The magnitude of this effect after 54 hours (at 0000 LST) and after 66 hours (at 1200 LST) of simulated time can be determined by comparing results from Runs 4 and 5 (Figs. 19 and 20). A net radiative cooling of about 5K resulted at all levels at both times. Both sets of profiles are nearly parallel, indicating that radiative flux divergence does not significantly affect PBL stability. Surface temperatures also show the effect of radiative cooling, as Run 5 values are also higher than the those of Run 4 by about 6K (Fig. 8).

Omission of radiative flux divergence does not significantly affect the diurnal cycle of u_* (Fig. 12), but Run 5 values are systematically lower (by a maximum difference of 10%) than those of Run 4, consistent with the slightly increased SBL stability of Run 5 (Fig. 13b). The difference

in R_i is small and nearly constant, but it indicates that radiative flux divergence contributes to a greater decrease in temperatures closer to surface than aloft.

Run 6 imposes a 6°C/day cooling at Ht upon the conditions of Run 1 (Table 1). The negative value of $\dot{\theta}_t$ produces a weaker subsidence velocity (Fig. 2), as ws(Ht) is defined by (2.14). The resulting downward vertical advection of this cooling air produces a surface cooling trend that lowers T_0 from its initial 26.3°C value to 6.7°C after 66 hours of simulated time (Figs. 7 and 8). The cooler surface yields high surface relative humidity values (Figs. 10 and 11).

The initial q(z) profile discontinuity at H_i was maintained until the end of the simulation (Fig. 21), albeit at a reduced magnitude and at the new lower H_i level. Above the inversion base, q-values remained constant, indicating a decoupling (because of the small diffusion term above H_i) from the PBL below.

At midnight on the final day of Run 6, a radiative surface based inversion does not occur, due to the high V_g value (Fig. 22). The base of the elevated subsidence inversion descended from its initial 450m to a height of 125m. Temperature increases 13K from the inversion base to its inversion top at 450m, defining a temperature gradient of

40K/km (about six times the upper boundary condition on $\dot{\theta}$). This unreasonably large gradient also occurred in Run 1 (Fig. 9), indicating that the effect is caused by the large values of w_s.

Cooling aloft (relative to changes at the surface) has the same destabilizing effect as surface warming, producing the consistently negative Run 6 SBL R_i values in Fig. 13b. The trend toward instability is due to the cold air source at the model top that continually propagates downward via subsidence.

Mechanical turbulence levels, parameterized by u_* (Fig. 12), are higher that those of Run 1. They also possess a slight increasing trend during the final 24 hours of the simulation (in association with the destabilizing SBL). The instability of this run produces K_θ values larger than those of Run 1 (Fig. 18), but smaller than those of Run 4, with its large constant H value.

As H is always given by Hi in Run 6, its value is grid level dependent, and its variation thus discrete (Figs. 5 and 6). Such jumps seldom occur, as they require model parameters to vary enough to induce a change in H_i of one grid level. During the final 48 simulated hours, H_i changed only

twice (Fig. 5). If the grid resolution was finer, more jumps would occur. Diurnal variations still arise, however, as surface convection dominates over subsidence, causing larger daytime than nighttime values.

Input values of τ, $\dot{\theta}_t$, and H_0 for Run 7 (Table 1 and Fig. 1) yield weaker (but more realistic) subsidence velocities than in Run 6 (Fig. 2). Subsidence inversion intensity thus weakens from its unrealistically large value in Run 6 (Fig. 22), while the intense mechanical mixing from the large value of V_g (Table 1) again inhibits formation of a midnight surface-based inversion. Values of H on the final day were higher for Run 7 than for all the other runs with subsidence (Fig. 6), as its weak (but non-zero) subsidence velocity and higher inversion base could not effectively cap daytime PBL growth.

The Run 7 surface temperature curve somewhat resembles that of Run 6 (Fig. 8), as there is no significant phase shift or amplitude variation among them. Differences include both its higher values and reduced daytime warming (due to downward advection of the imposed larger model-top cooling rate). Surface relative humidity values for Run 7 (Fig. 11) were, however, higher than those of Run 6, and close to 100% at 0600 LST. This resulted as the initial Run 7 moist sub-inversion PBL layer was deeper than in Run 6

(Fig. 1). Thus the enhanced downward advection of moisture was a more important positive influence on surface relative humidity than the negative influence of its increased surface temperatures.

The diurnal cycle of Run 7 SBL Ri is also similar to that of Run 6 (Fig. 13b). Its reduced daytime instability results from the reduced daytime warming discussed above. Run 7 friction velocity values were larger than those of Run 6 (Fig. 23), consistent with its less unstable SBL R_i values.

The Run 8 V_g speed value is reduced to 4m/s (Table 1). As the initial inversion height is also increased for this case (relative to Run 1), its subsidence velocity is weaker at lower levels than for Run 1 (Fig. 2).

Resulting reduced mechanical friction values (Fig. 23) allowed a nocturnal surface radiation inversion to form (Fig. 22). Inversion intensity at 0000 LST also reflects the weaker subsidence, i.e., the exaggerated low level Run 1 layer is replaced by a more reasonable weaker elevated layer in Run 8.

The temporal variation of Run 8 H values resembles that of Run 2 (Fig. 6). The low V_g speed for Run 8, and the

omission of subsidence in Run 2, each allows daytime heat convection to overcome the effect of subsidence, allowing H to increase. The subsidence in Run 8, however, causes lower H values than in the no-subsidence Run 2 case.

5. CONCLUSION

A one-dimensional version of the three-dimensional URBMET planetary boundary layer (PBL) model has been modified to more realistically simulate vertical PBL structure over homogeneous terrain. Time varying PBL heights were included, and its new initial conditions include a large scale subsidence inversion with an associated subsidence velocity profile. Subsidence magnitude at the model top was evaluated using a new upper boundary condition on potential temperature consistent with the imbalance between the various large scale and mesoscale forcings.

Simulations using time varying PBL heights with the large scale subsidence produced more realistic results, e.g., simulated shallower nighttime than daytime H(t) values produced realistically smaller nighttime than daytime, O'Brien (1970), diffusivity values. Nighttime temperature profiles also improved, e.g., a realistic elevated mixing layer inversion was not produced in experiments in which H was held constant at large values typical of daytime conditions.

Results showed that subsidence velocity was necessary to sustain the initial elevated inversion against surface convective effects. The model was sensitive to subsidence

magnitude, e.g., when overestimated, elevated inversion strength was overestimated.

Imposed cooling at the model top propagated down to the surface via advection, causing a cooling trend upon which was superimposed the normal diurnal surface temperature cycle. Such cooling also produced an unstable SBL throughout the entire diurnal cycle.

An initial adjustment period for H(t) occurred, indicating the need for a new equilibrium phase within the current initialization procedure. This would allow the subsidence velocity and temperature profiles to achieve equilibrium before starting the main simulation.

Temperature profiles on the final simulated day show an unrealistic steady state near-neutral layer above the subsidence inversion top. The steady-state upper inversion lapse rate boundary condition thus becomes inconsistent with this layer. The upper boundary condition on θ should thus be redefined to avoid this inconsistency. One possibility (at each time step) is to set the lapse rate at the model top equal to that predicted at the grid point below it, producing consistency between the two levels. This problem does not, however, adversely effect the more important results within and below the inversion.

An improved imposed external larger scale subsidence velocity profile is also necessary; this can be obtained from appropriate field observations in the literature. Additional model grid points at the higher levels would permit a finer resolution of elevated subsidence inversion characteristics and PBL heights. Such improvements should yield more realistic interactions between large scale and mesoscale effects within and above the PBL.

REFERENCES

Arya, S.P.S., and D.W. Byun, 1985: Rate equations for the PBL depth (urban vs rural). Dept. of Marine, Earth and Atmospheric Sciences, North Carolina State Univ., 30 pp.

Anthes, R.A., and T.T. Warner, 1978: Development of hydrodynamic models suitable for air pollution and other mesometeorological studies. Mon. Wea. Rev., 106, 1045-1099.

Barnum, D.C., and G.V. Rao, 1975: Role of advection and penetrative convection in affecting the mixing-height variations over an idealized metropolitan area. Boundary Layer Meteor., 8, 497-514.

Bengtsson, L., M. Ghil, and E. Kallen, 1981: Dynamic meteorology: data assimilation methods. Springer-Verlag, Inc., New York, 330 pp.

Blackadar, A.K., 1962: The vertical distribution of wind and turbulent exchange in a neutral atmosphere. J. Geophys. Res., 67, 3097-3102.

Blackadar, A.K., and H. Tennekes, 1968: Asymptotic similarity in neutral barotropic planetary layer. J. Atmos. Sci., 25, 1015-1020.

Bornstein, R.D., 1975: The two-dimensional URBMET urban boundary layer model. J. Appl. Meteor, 14(8), 1459-1477.

Bornstein, R.D., and A.D. Robock, 1976: Effects of variable and unequal advection and diffusion time steps in the simulation of an urban boundary layer. Mon. Wea. Rev., 104, 260-267.

Bornstein. R.D., and E. Runca, 1977: Preliminary investigations of sulfur dioxide patterns in Venice, Italy using linked PBL and K-models, including removal processes. Proc. Joint Conf. on Applications of Air Pollution Meteorology, Nov. 22-Dec. 2, 1977 Salt Lake City, UT: Amer. Meteor. Soc. and Air Poll. Contr. Assn., 277-282.

Bornstein, R.D., S. Klotz, R. Street, U. Pechinger, and R. Miller, 1987: Modeling the polluted coastal urban environment. volume I: The PBL model. EPRI Report for Contract No. 1630-13.

Brost R.A., and J.C. Wyngaard 1978: A model of the stably stratified planetary boundary layer. J. Atmos. Sci. 35, 1427-1440.

Businger, J.A., J.C. Wyngaard, Y. Izumi, and E.F. Bradley, 1971: Flux profile relationships in the atmospheric surface layer. J. Atmos. Sci., 28, 181-189.

Cederwall, R.T., 1980: Effect of long wave radiative cooling on west coast subsidence inversions under cloudless conditions. M.S. Thesis, Dept. of Meteorology, San Jose State Univ., 65 pp.

Clarke, R.H., A.J. Dyer, R.R. Brook, D.G. Reid, and A.J. Troup, 1971: The Wangara experiment: boundary layer data. CSIRO Div. of Meteorol.Phys.Tech. Paper No.19, 340 pp.

Deardorff, J., 1974:Three-dimensional numerical study of the height and mean structure of a heated planetary boundary layer. Boundary Layer Meteor., 7, 81-106.

Deardorff, J.W., G.E. Willis, and D.K Lilly, 1974: Comment on the paper by A.K. Betts: "Non -Precipitating Cumulus Convection and Its Parameterization". Quart.J. Roy. Meteorol. Soc., 100, 122-123.

Diertele, D., 1979: Simulation of the urban surface energy balance, including the effects of anthropogenic heat production. M.S. Thesis, Dept. of Meteorology, San Jose State Univ., 65 pp.

Estoque, M.A., 1961: A theoretical investigation of the sea breeze. Quart. J. R. Meteor. Soc., 87, 136-146.

Estoque, M.A., 1962: The sea breeze as a function of the prevailing synoptic situation. J. Atmos. Sci., 19, 244-250.

Garratt, J.R., 1982: Surface fluxes and the nocturnal boundary layer height. J. Appl. Meteor., 21, 725-729.

MacCracken M.C., and R.D. Bornstein, 1977: On the treatment of advection in flux formulations with application to two models of the atmosphere. J. Comp. Phys. 23, No. 2, 135-149.

Mahrt, L., J.C. Andre, and R. C. Heald, 1982: On the depth of the nocturnal boundary layer. J. Appl. Meteor., 21, 90-92.

Melgarejo, J.W., and J.W. Deardorff, 1975: Revision to stability functions for the boundary-layer resistance laws based upon observed boundary layer heights. J. Atmos. Sci., 32, 837-839.

Nieuwstadt, F.T.M. 1984a: A Model for the stationary, stable boundary layer. Proceedings of the Conference on Models of Turbulence and Diffusion in Stably Stratified Regions of the Natural Environment, March 1983, Cambridge, 149-179.

Nieuwstadt, F.T.M. 1984b: Some aspects of the turbulent stable boundary layer. Boundary Layer Meteor., 30, 31-35.

O'Brien, J., 1970: On the vertical structure of eddy exchange coefficient in the planetary boundary layer. J. Atmos. Sci., 27, 1213-1215.

Pielke, R.A., 1974: A three-dimensional numerical model of the sea breezes over south Florida. Mon. Wea. Rev., 102, 115-139.

Pielke, R.A., and Y. Mahrer, 1975: Representation of the heated planetary boundary layer in mesoscales models with coarse vertical resolution. J. Atmos. Sci., 32, 2288-2308.

Pielke, R.A., 1984: Mesoscale Meteorological Modeling. Academic Press, Inc., Orlando, 612 pp.

Reichenbacher, W., and R.D. Bornstein, 1979: Experiments with time and space varying upper boundary conditions in a PBL model. Preprint volume of Fourth Symposium on Turbulence, Diffusion, and Air Pollution, Jan. 15-18, 1979, Reno, Nevada, 483-489.

Reuter H., 1987: Personal communication.

Santhanam, K., 1980: One-dimensional simulation of temperature and moisture in atmospheric and soil layers. M.S. Thesis, Dept. of Meteorology, San Jose State Univ., 89 pp.

Sasaki, Y. 1970: Some basic formalisms in numerical variational analysis. Mon. Wea. Rev., 98, 875-883.

Sasamori, T. 1970: A numerical study of atmospheric and soil boundary layers. J. Atmos. Sci., 27, 1122-37.

Segal, M., and R.A. Pielke, 1981: Numerical model simulation of biometeorological heat load condition summer day case study for the Chesapeake Bay area. J. Appl. Meteorol. 20. 735-749.

Segal, M., R.T. McNider, R.A. Pielke, and D.S. McDougal 1982: A numerical model simulation of the regional air pollution meteorology of the greater Chesapeake bay area - Summer day case study. Atmos.Env., 16, 1381-1397.

Yamada T., and G. Mellor, 1975: A simulation of the Wangara atmospheric boundary layer data. J. Atmos. Sci., 32, 2309-2329.

Yu, T., 1978: Determining height of the nocturnal boundary layer. J. Appl. Meter., 17, 28-33.

Zilitinkevich, S.S., 1970: Dynamics of atmospheric boundary layer. Gidrometeoizdat, Leningrad.

Zilitinkevich, S.S., 1972: On the determination of the height of the Ekman boundary layer. Boundary Layer Meteor., 3, 141-145.

APPENDIX: NOMENCLATURE

Roman letters:

a	Ekman wind profile parameter
c	constant in PBL depth equation
c_p	specific heat of dry air
f	Coriolis parameter
g	acceleration due to gravity
H	PBL depth
H_c	analytical mixing or mixed layer depth
H_i	base of elevated inversion
H_t	transition layer top
H_0	initial base of elevated inversion
h	SBL depth
I	scale analysis ratio
K	vertical transfer coefficient
k	vertical unit vector
k_0	von Karman constant
L	Monin-Obukhov length
Q	radiative flux divergence
Q_L	long wave radiative flux divergence
Q_N	net radiative flux divergence
q	specific humidity
R	ideal gas constant
RH	surface relative humidity

R_i	Richardson number
R_{if}	flux Richardson number
T	temperature
T_d	dew point temperature
T_0	surface temperature
T_*	scale temperature
t	time
t_1	time before model initialization
t_2	time of model initialization
U	scale horizontal synoptic wind speed
u, v, w,	component of wind in x, y, and z-directions, respectively
u_*	horizontal friction velocity
V	horizontal wind speed
V	horizontal wind velocity
w_*	convective velocity
x, y, z	horizontal and vertical coordinate direction
z_0	surface roughness

Greek letters

α	cross isobar flow angle
$\Delta()$	difference operator
τ	initial gradient of potential temperature within elevated inversion
Γ	dry adiabatic cooling rate

$\tilde{\tau}$	inertial period
ϕ	latitude angle
ρ	atmospheric density
θ	potential temperature
θ_0	surface potential temperature
θ_*	friction potential temperature
Ω	angular velocity of earth

Subscripts and superscripts

$()_a$	volume average
$()_g$	geostrophic value
$()_\theta$	heat
$()_h$	at h
$()_m$	momentum
$()^n$	value at timestep n
$()_s$	synoptic scale value
$()_k$	grid level index
$()_t$	at model top
$()^+$	value above H
$\dot{()}$	local rate of change

LIST OF FIGURES

Figure 7. Time variation of surface temperature for Runs 1 (pluses), 3 (asterisks), and 6 (dots) over entire 72 hour simulation, where initial time is 1800 LST.

Figure 8. Time variation of surface temperature for Runs 1 (pluses), 2 (asterisks), 3 (squares), 4 (xes), 5 (diamonds), 6 (dots), and 7 (triangles) for the final simulation day, where initial time is 1800 LST.

Figure 9. Temperature profiles for Run 1 at 2000 (dots), 0000 (pluses), 0800 (asterisks) and 1200 (squares) LST on the final simulation day, where initial time is 1800 LST; also shown is dry adiabatic lapse rate Γ_D.

Figure 10. Time variation of surface relative humidity for Runs 1 (pluses), 3 (asterisks), and 6 (dots) over entire 72 hour simulation, where initial time is 1800 LST.

Figure 11. Time variation of surface relative humidity for Runs 1 (pluses), 2 (asterisks), 6 (dots), and 7 (squares) for the final simulation day, where initial time is 1800 LST.

Figure 12. Time variation of friction velocity u_* for Runs 1 (pluses), 2 (squares), 3 (dots), 4 (xes), 5 (diamonds), and 6 (asterisks) for the final simulation day, where initial time is 1800 LST.

Figure 13a. Time variation of SBL Richardson number Ri for Runs 1 (pluses), 2 (diamonds), 3 (xes), and 4 (triangles) for the final simulation day, where initial time is 1800 LST.

Figure 13b. Time variation of SBL Richardson number Ri for Runs 5 (asterisks), 6 (dots), and 7 (squares) for the final simulation day, where initial time is 1800 LST.

Figure 14. Heat diffusivity profiles for Run 1 at 2000 (dots), 0000 (xes), and 0800 (asterisks), and 1200 (squares) LST on the final simulation day, where initial time is 1800 LST.

Figure 15. Time variation of PBL depth for Runs 2 (asterisks) and 3 (squares) for the final simulation day, where initial time is 1800 LST.

Figure 16. Run 3 specific humidity q, temperature T, and potential temperature θ profiles at 0000 LST on the final simulation day; also shown is dry adiabatic lapse rate Γ_D.

Figure 17. Run 3 specific humidity q, temperature T, and potential temperature θ profiles at 1200 LST on the final simulation day; also shown is dry adiabatic lapse rate Γ_D.

Figure 18. Heat diffusivity profiles for Runs 1 (dots), 4 (asterisks), and 6 (squares) at 0000 LST on the final simulation day, where initial time is 1800 LST.

Figure 19. Temperature T profiles for Runs 4 (asterisks) and 5 (dots) at 0000 LST on the final simulation day; also shown is dry adiabatic lapse rate Γ_D.

Figure 20. Temperature profiles for Runs 4 (squares) and 5 (pluses) at 1200 LST on the final simulation day; also shown is dry adiabatic lapse rate Γ_D.

Figure 21. Run 6 specific humidity q, temperature T, and potential temperature θ profiles at 1200 LST on the final simulation day; also shown is dry adiabatic lapse rate Γ_D.

Figure 22. Temperature T profiles for Runs 6 (dots), 7 (pluses), and 8 (asterisks) at 0000 LST on the final simulation day; also shown is dry adiabatic lapse rate Γ_D.

Figure 23. Time variation of friction velocity u_* for Runs 1 (pluses), 6 (asterisks), 7 (triangles), and 8 (diamonds) for the final simulation day, where initial time is 1800 LST.

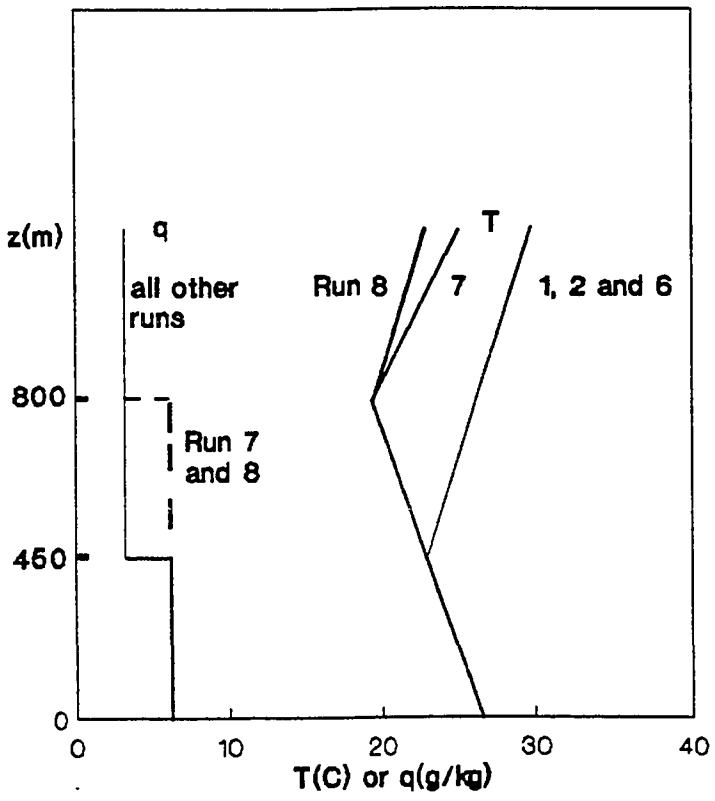
z(m)
q
all other runs
Run 7 and 8
800
450
0
T
Run 8
7
1, 2 and 6
0
10
20
30
40
T(C) or q(g/kg)

Fig. 1

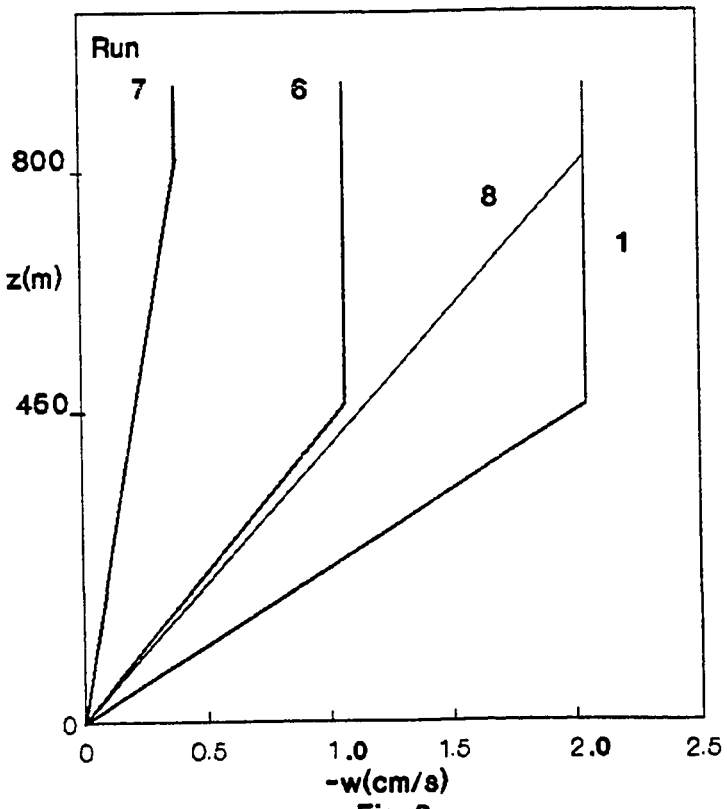

Fig. 2

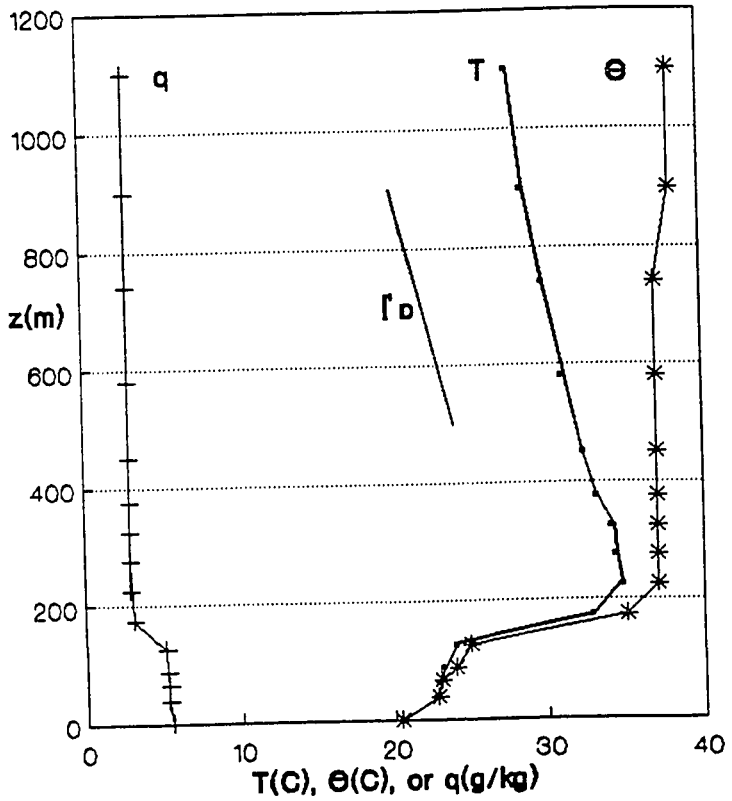

Fig. 3

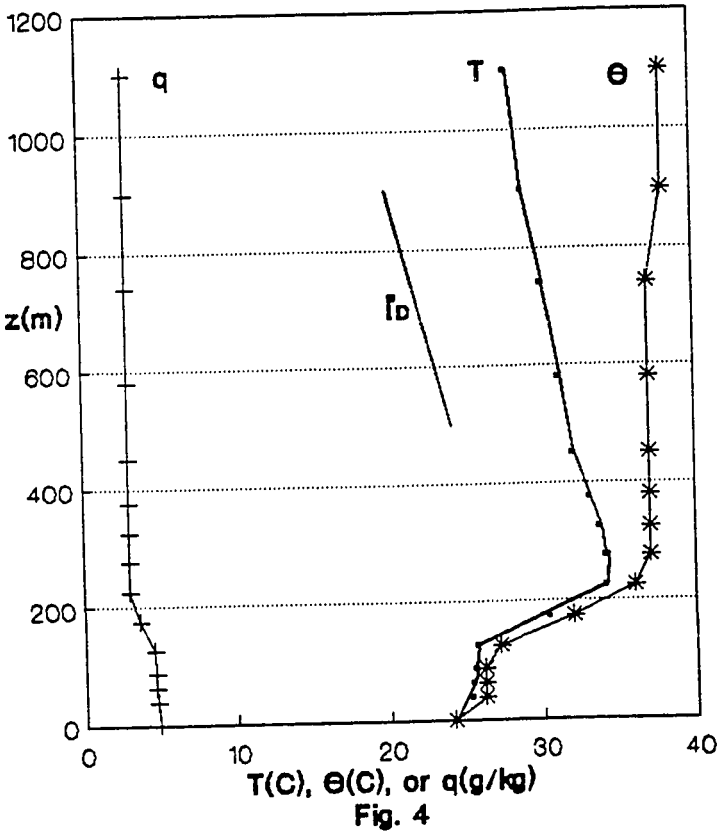

Fig. 4

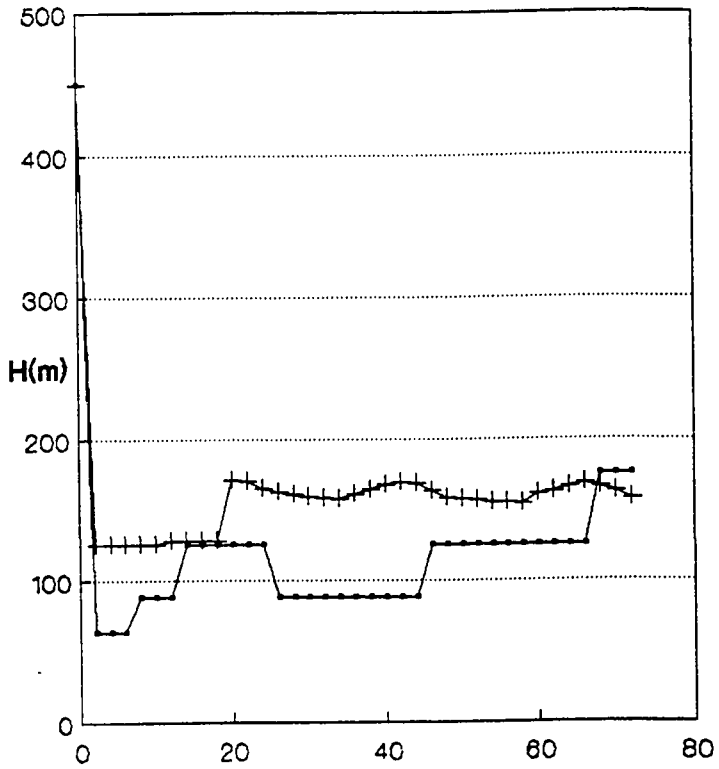

Fig. 6

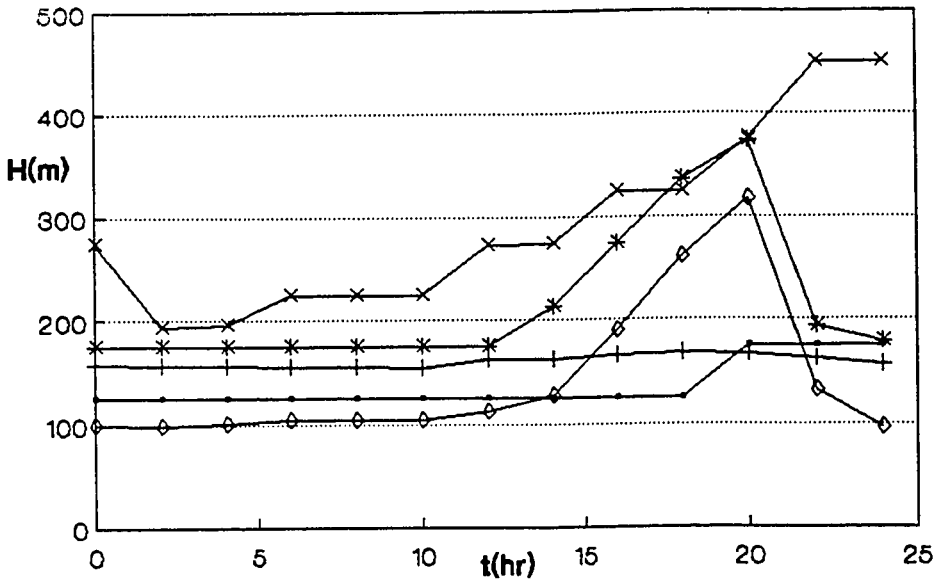

Fig. 6

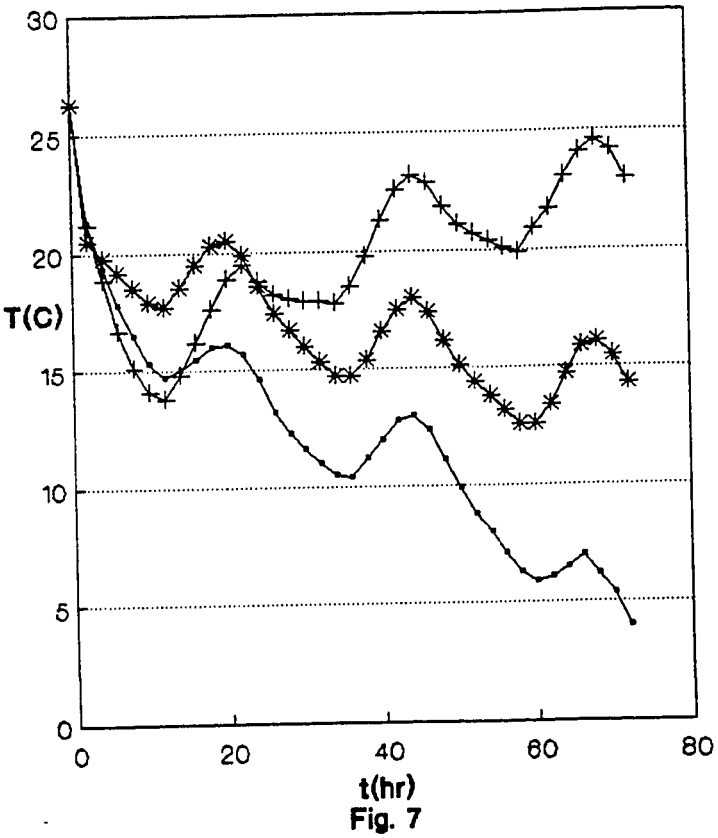

Fig. 7

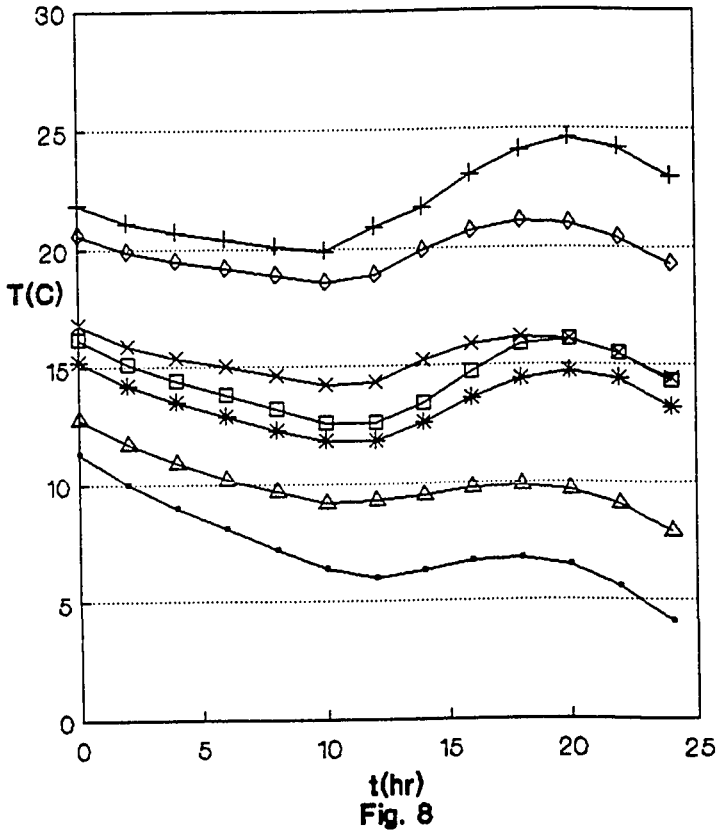

Fig. 8

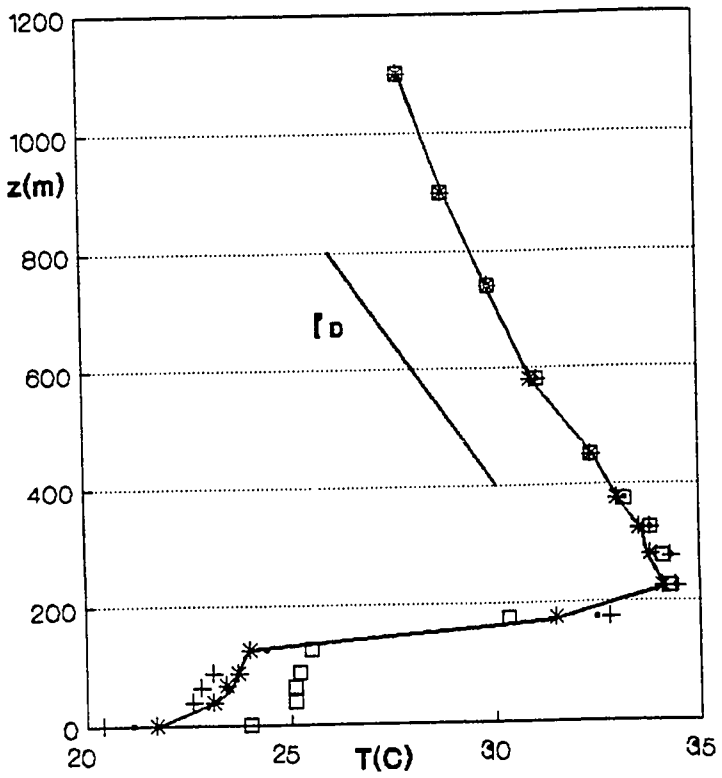

Fig. 9

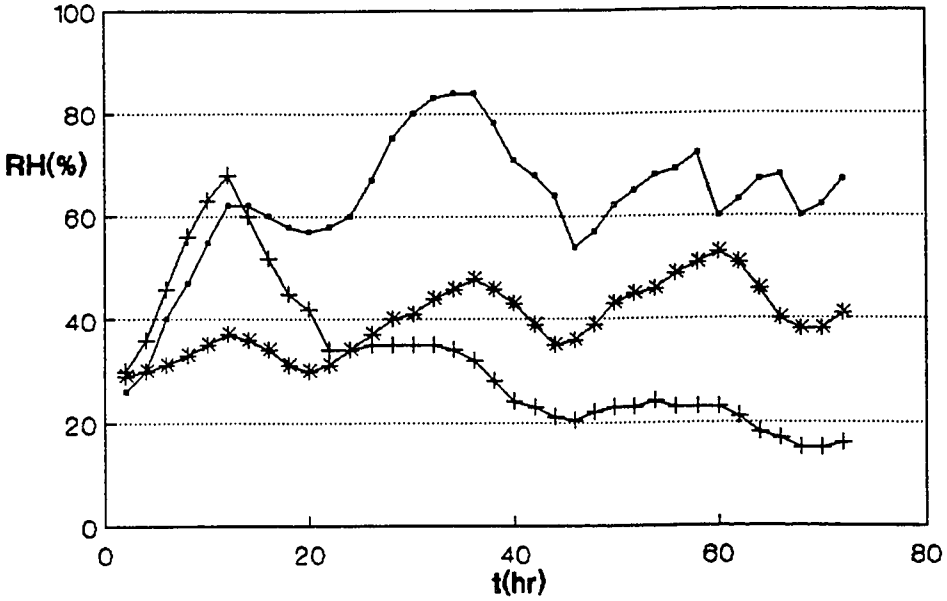

Fig. 10

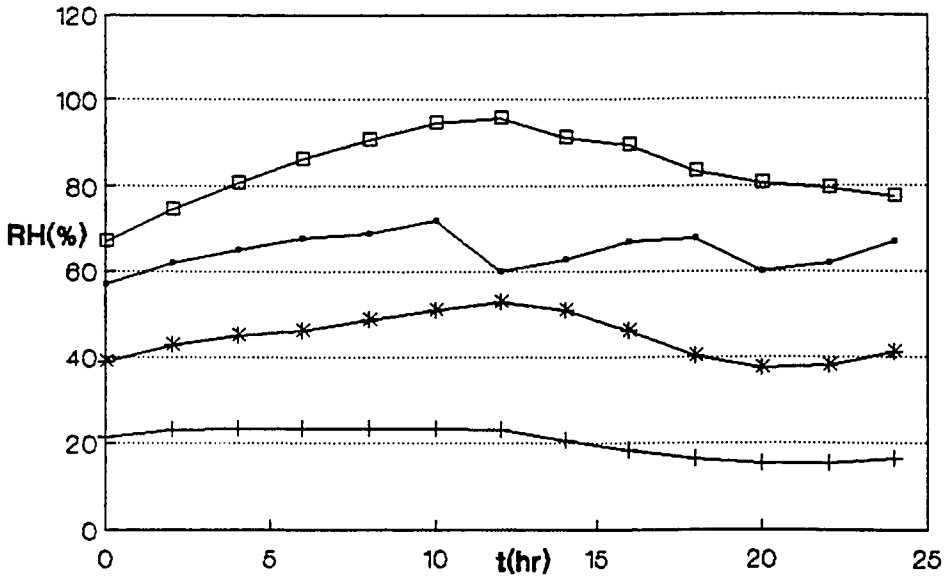

Fig. 11

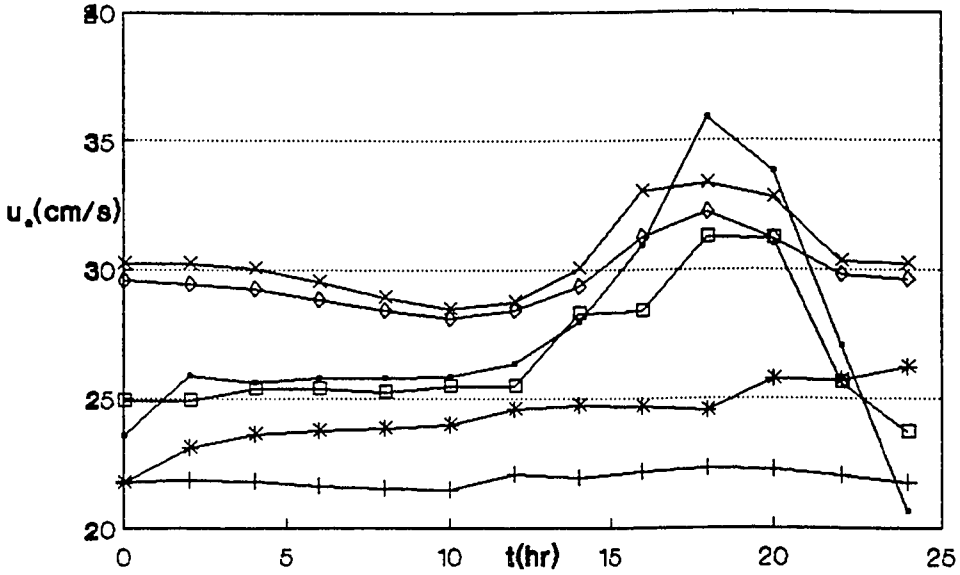

Fig. 12

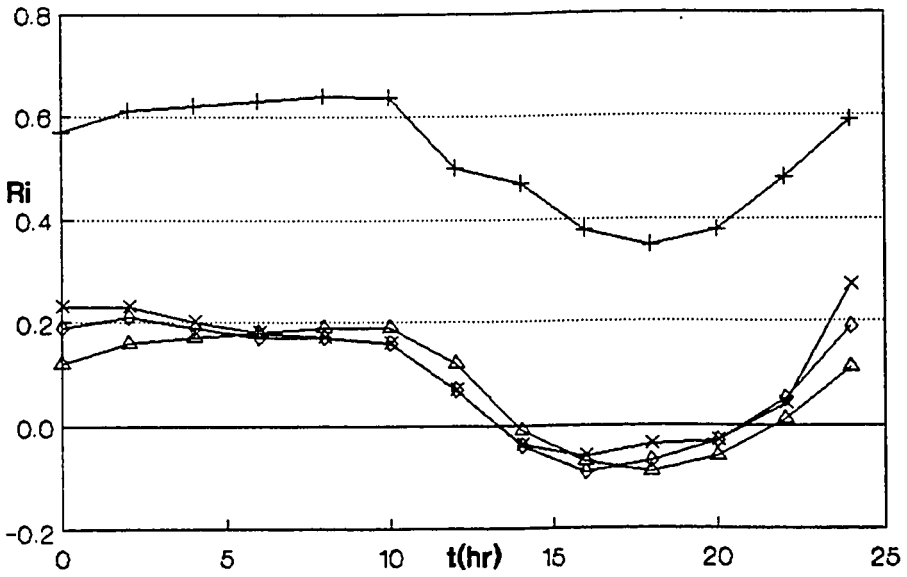

Fig. 13a

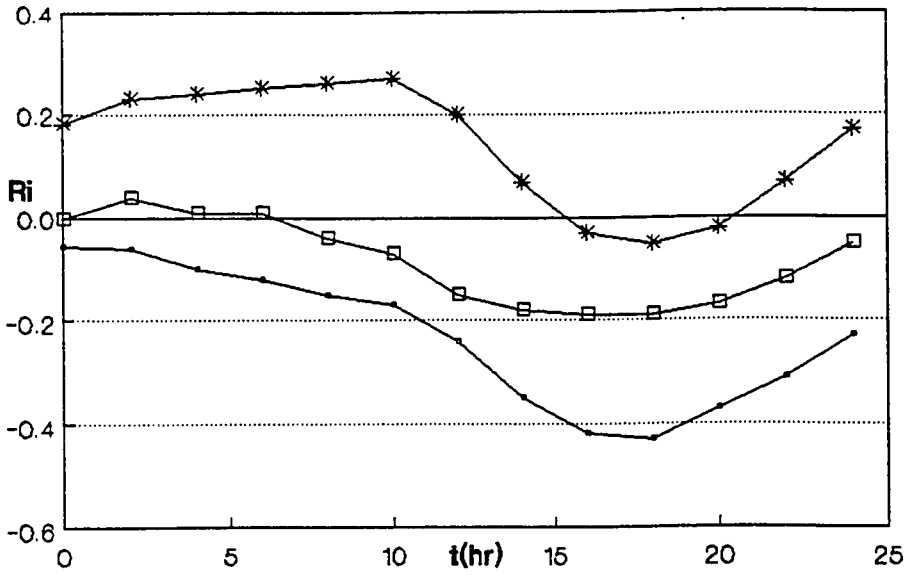

Fig. 13b

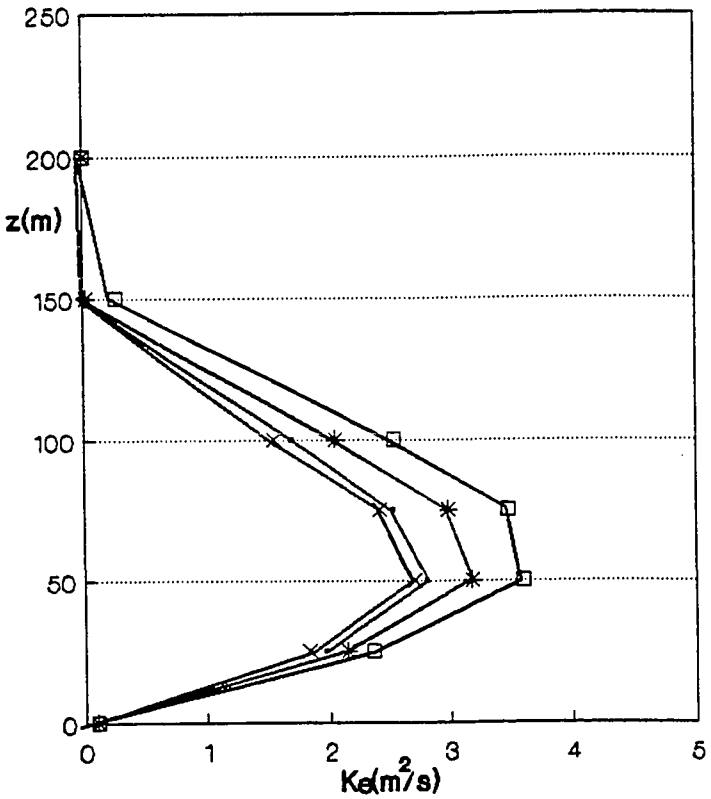

Fig. 14

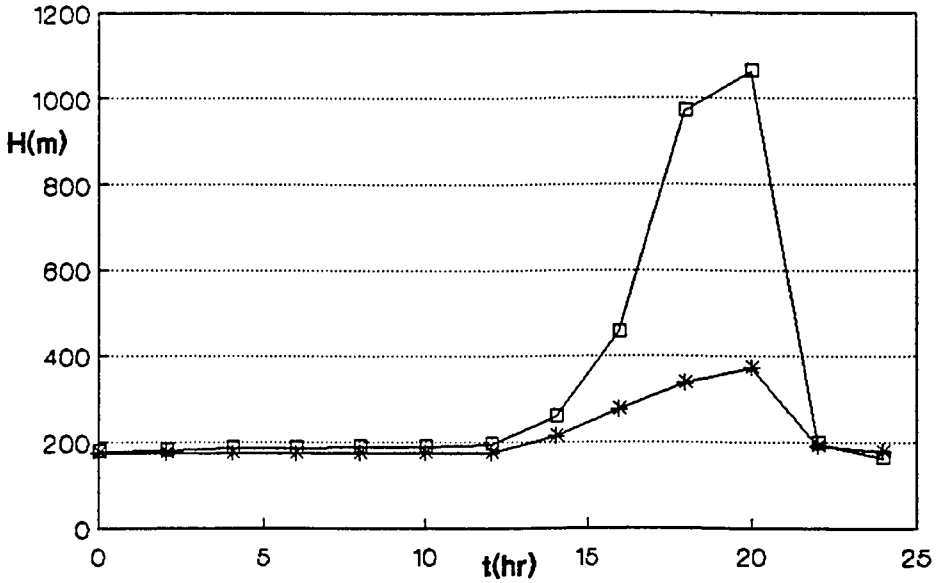

Fig. 15

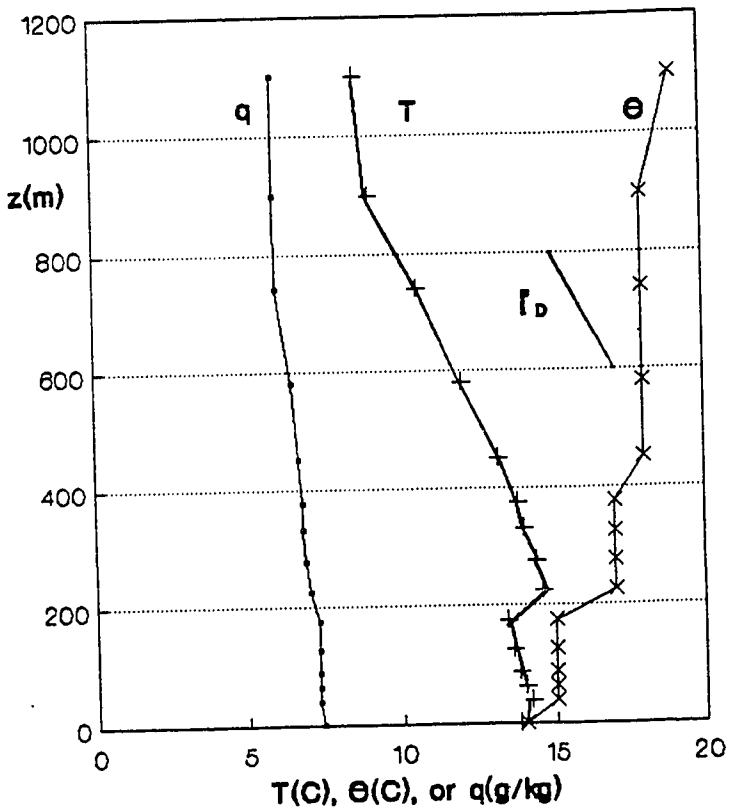

Fig. 16

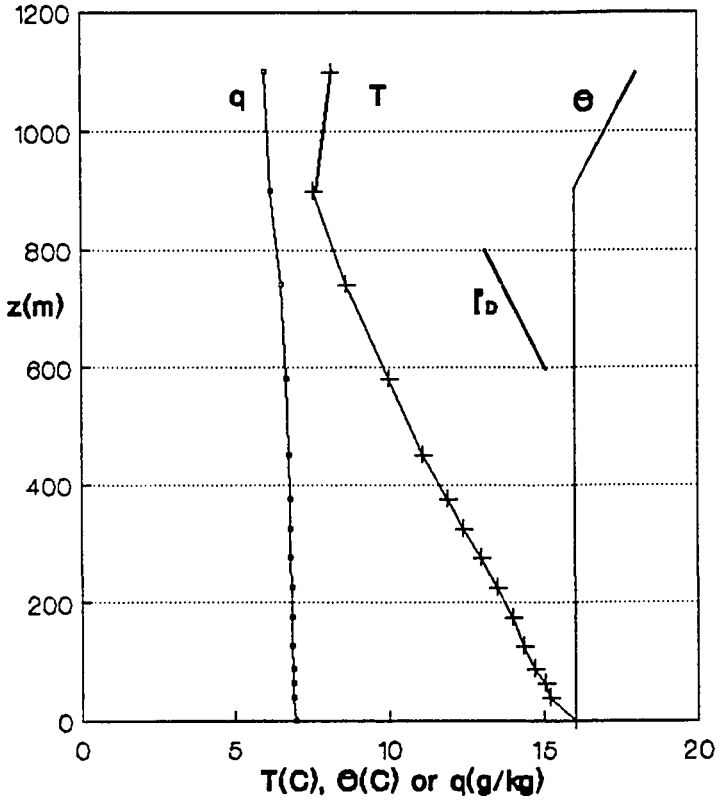

Fig. 17

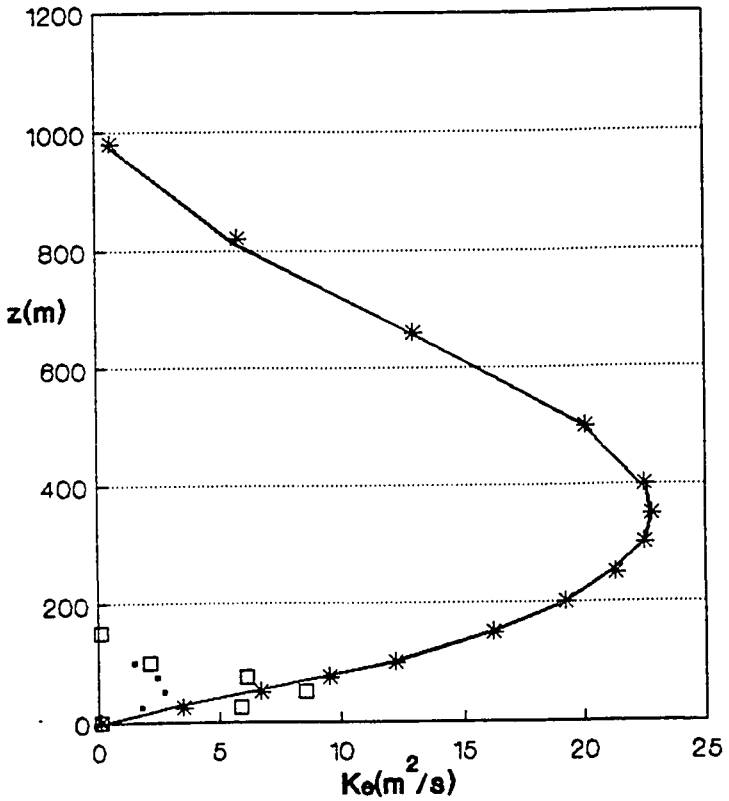

Fig. 18

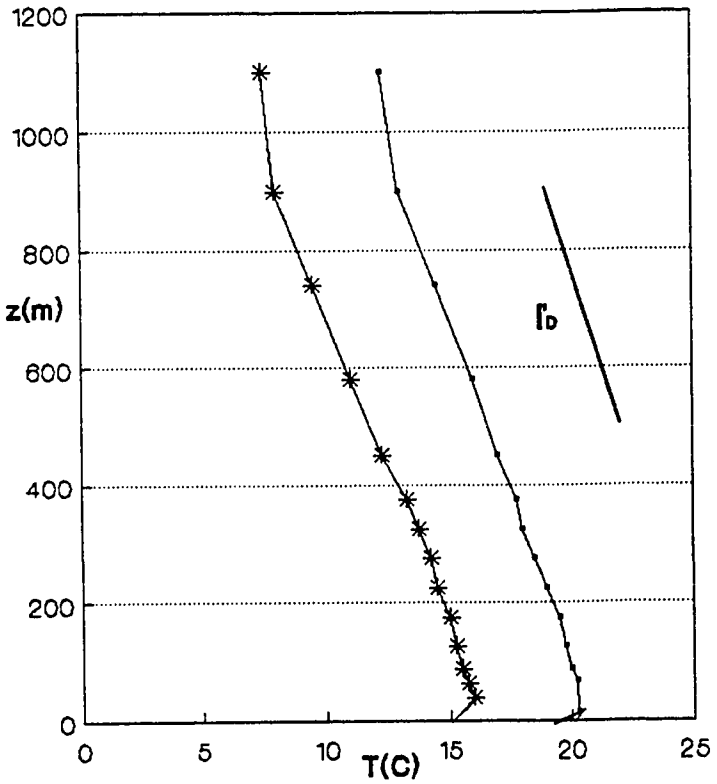

Fig. 19

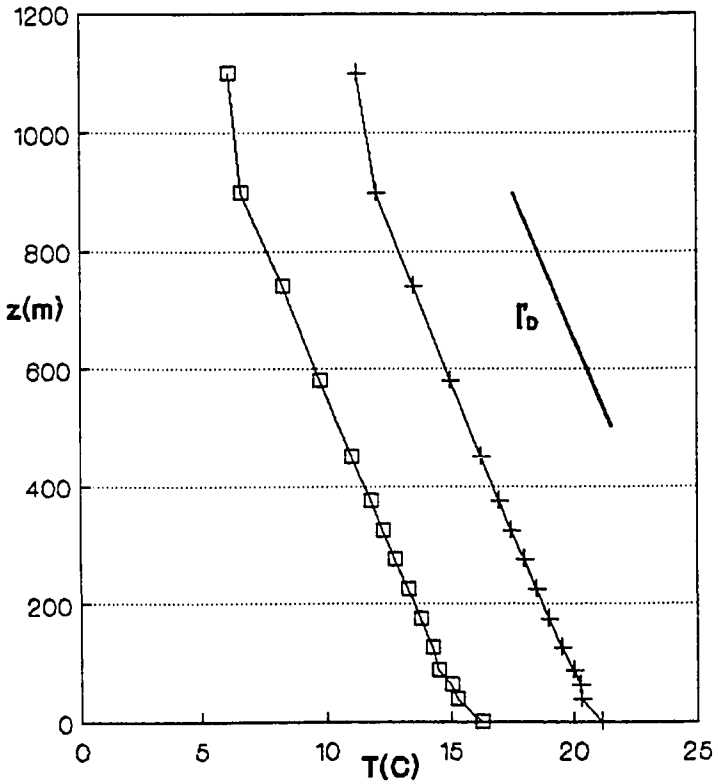

Fig. 20

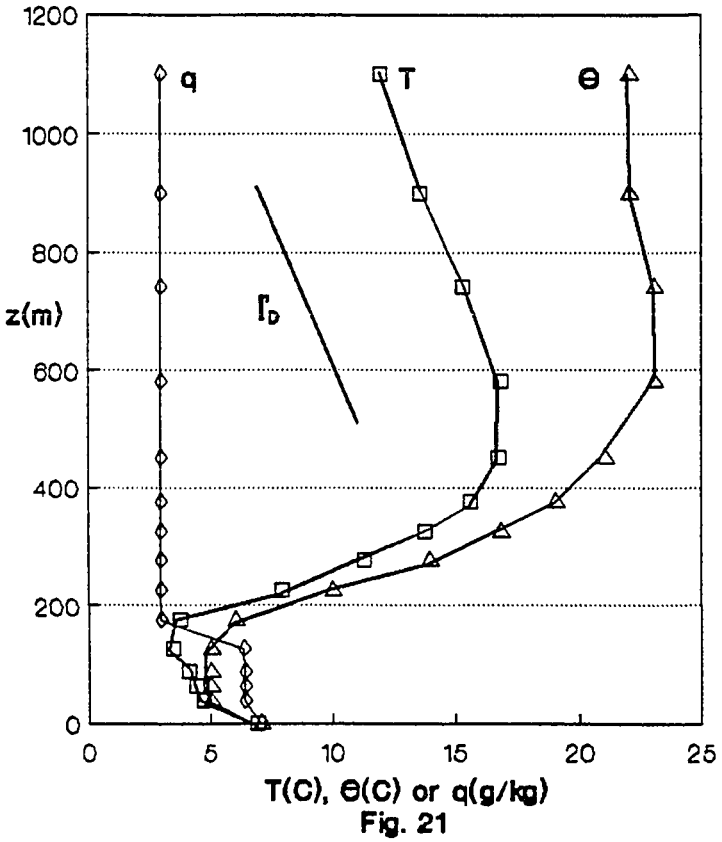
1200
1000
800
600
400
200
0
z(m)
q
T
θ
Γ_D
0
5
10
15
20
25
T(C), θ(C) or q(g/kg)
Fig. 21

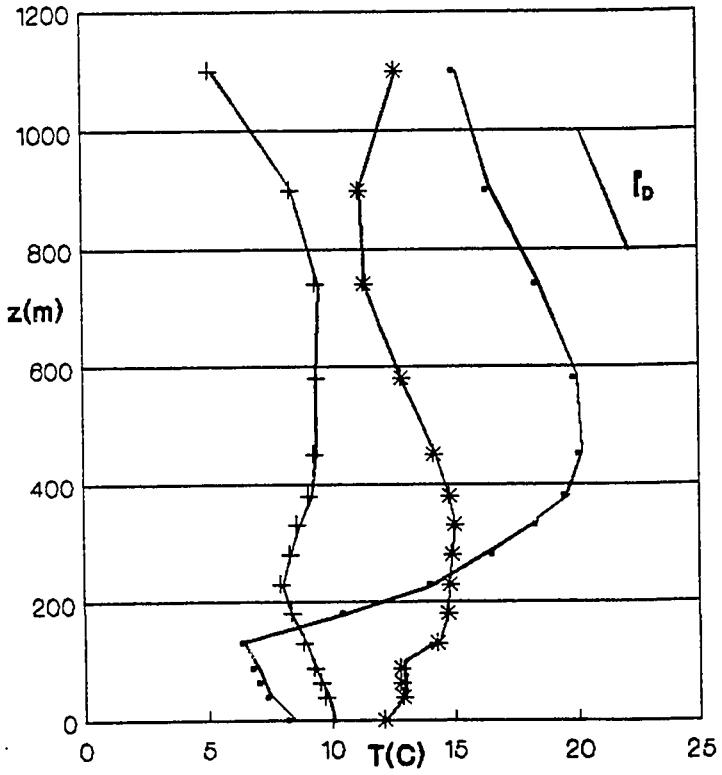

Fig. 22

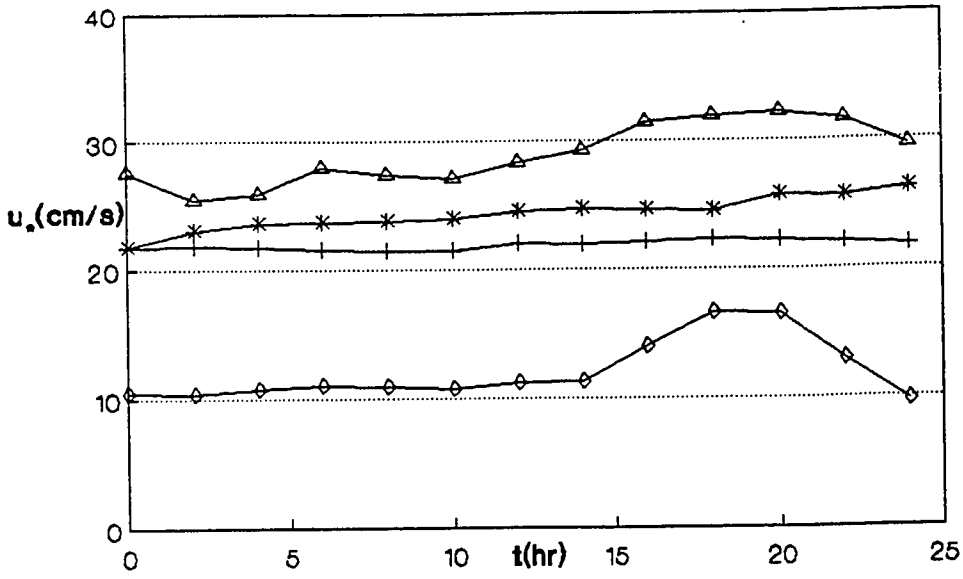

Fig. 23